I. GLOBAL PARTON ANALYSES

The calculation of the production cross sections at the LHC for both interesting physics processes and their backgrounds relies upon a knowledge of the distribution of the momentum fraction x of the partons in a proton in the relevant kinematic range. [1] These parton distribution functions (pdf's) are determined by global fits to data from deep inelastic scattering (DIS), Drell-Yan (DY), and jet and direct photon production at current energy ranges. Two major groups, CTEQ [2] and MRS [3], provide semi-regular updates to the parton distributions when new data and/or theoretical developments become available.

Lepton-lepton, lepton-hadron and hadron-hadron interactions probe complementary aspects of perturbative QCD (pQCD). Lepton-lepton processes provide clean measurements of $\alpha_s(Q^2)$ and of the fragmentation functions of partons into hadrons. Measurements of deep-inelastic scattering (DIS) structure functions (F_2, F_3) in lepton-hadron scattering and of lepton pair production cross sections in hadron-hadron collisions provide the main source on quark distributions $f^a(x,Q)$ inside hadrons. At leading order, the gluon distribution function g(x,Q) enters directly in hadron-hadron scattering processes with direct photon and jet final states. Modern global parton distribution fits are carried out to next-to-leading (NLO) order which allows $\alpha_s(Q^2), q^a(x,Q)$ and $g(x,Q)$ to all mix and contribute in the theoretical formulae for all processes. Nevertheless, the broad picture described above still holds to some degree in global pdf analyses. In pQCD, the gluon distribution is always accompanied by a factor of α_s, in both the hard scattering cross sections and in the evolution equations for parton distributions. Thus, determination of α_s and the gluon distribution is, in general, a strongly coupled problem. One can determine α_s separately from e^+e^- or determine α_s and $g(x,Q)$ jointly in a global pdf analysis. In the latter case, though, the coupling of α_s and the gluon distribution may not lead to a unique solution for either. (See for example the discussion in the CTEQ4 paper. [4])

Currently, the world average value of $\alpha_s(M_Z)$ is on the order of 0.118-0.119 [5] The average value from LEP is .121 while the DIS experiments prefer a somewhat smaller value (of the order of 0.116-0.117). Since global pdf analyses are dominated by the high statistics DIS data, they would tend to favor the values of α_s closer to the lower DIS values. The more logical approach is to adopt the world average value of $\alpha_s(M_Z)$ and concentrate on the determination of the pdf's. This is what both CTEQ and MRS currently do.

The data from DIS, DY, direct photon and jet processes utilized in pdf fits cover a wide range in x and Q. The kinematic "map" in the (x,Q) plane of the data points used in a recent parton distribution function analyses is shown in Figure 1. The HERA data (H1+ZEUS) are predominantly at low x, while the fixed target DIS and DY data are at higher x. There is considerable overlap, however, with the degree of overlap increasing with time as the statistics of the HERA experiments increases. DGLAP-based NLO pQCD should provide an accurate description of the data (and of the evolution of the parton distributions) over the entire kinematic range shown. At very low x and Q, DGLAP evolution is believed to be no longer applicable and a BFKL description must be used. No clear evidence of BFKL physics is seen in the current range of data; thus all global analyses use conventional DGLAP evolution of pdf's.

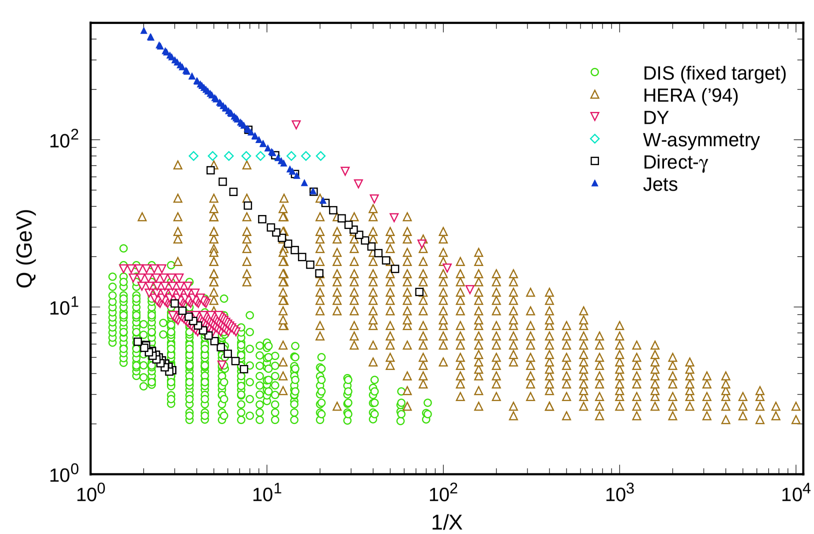

FIG. 1. The kinematic map in the (x,Q) plane of data points used in the CTEQ5 analysis.

There is a remarkable consistency between the data in the pdf fits and the NLO QCD theory fit to them. Over 1300 data points are shown in Figure 1 and the χ^2/DOF for the fit of theory to data is on the order of 1.

The parton distributions from the recent CTEQ pdf release are plotted in Figure 2 at a Q value of 5 GeV. The gluon distribution is dominant at x values of less than .01 with the valence quark distributions dominant at higher x.

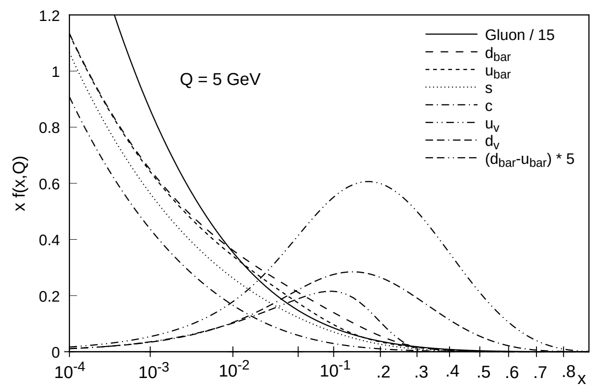

FIG. 2. The parton distributions from the CTEQ5 set plotted at a Q value of 5 GeV.

For comparison purposes, the kinematics appropriate for the production of a state of mass M and rapidity y at the LHC is shown in Figure 3. [6] For example, to produce a state of mass 100 GeV and rapidity 2 requires partons of x values .05 and .001 at a Q^2 value of $1X10^4\ GeV^2$. Also shown in the figure is another view of the kinematic coverage of the fixed target and HERA experiments used in pdf fits.

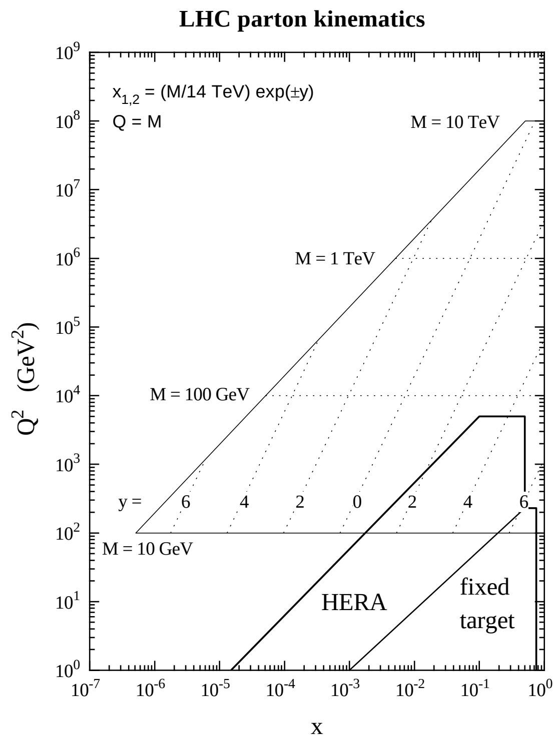

FIG. 3. A plot of LHC parton kinematics in (x, Q^2) space. Also shown are the reach of fixed target and HERA experiments.

II. EVOLUTION

Parton distributions determined at a given x and Q^2 "feed-down" to lower x values at higher Q^2 values. The accuracy of the extrapolation to higher Q^2 depends both on the accuracy of the original measurement and any uncertainty on $\alpha_s(Q^2)$.* For the structure

*The evolution can be carried out in either moment space or configuration space. Current programs in use by CTEQ and MRS should be able to carry out the evolution using NLO DGLAP to an accuracy of a few percent over the LHC kinematic range, except perhaps at large x. Evolution programs at NNLO may be available at the time of the LHC turnon, but the advantages over NLO evolution should be minimal.

function F_2, the typical measurement uncertainty at medium to large x is on the order of $\pm3\%$. At large x, the DGLAP equation for F_2 can be approximated as $\frac{\partial F_2}{\partial \log\ Q^2} = \alpha_s(Q^2)P^{qq}\otimes F_2$. The effect on the evolution of a world average of α_s and its error ($\alpha_s(M_Z^2) = 0.1175 \pm 0.005$) is shown in Figure 4. [6] There is an extrapolation uncertainty of $\pm5\%$ in F_2 at high Q^2 ($10^5 GeV^2$) from the given uncertainty in α_s.

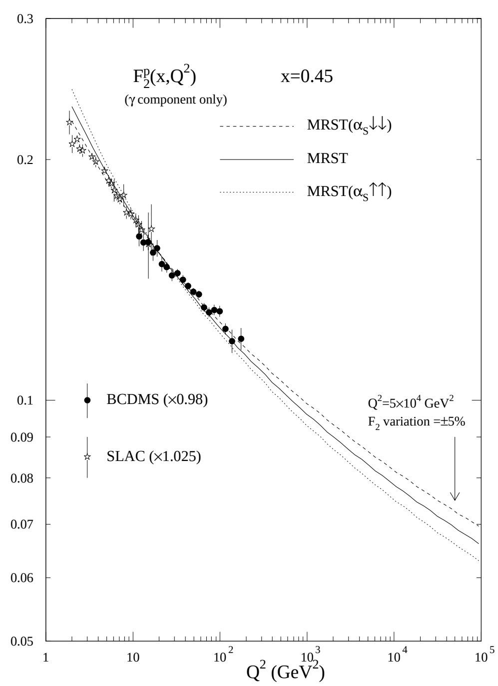

FIG. 4. The extrapolation of the fits at $x = 0.45$ to high Q^2 using the main MRST pdf ($\alpha_s(M_Z) = 0.1175$) and the MRST pdf's corresponding to the upper (.1225) and lower (.1125) range of uncertainty on $\alpha_s(M_Z)$.

The effects of evolution are examined in more detail in Figure 5 where the gluon distribution is plotted at Q^2 values of 2, 10, 50, 10^4 and $10^6 GeV^2$. There are two interesting features that can be noted. Most of the evolution takes place at low Q^2 and there is little evolution for x values in the vicinity of 0.1. In contrast, at an x value of 0.5, the gluon distribution decreases by a factor of approximately 30 from the lowest to the highest Q^2 value.

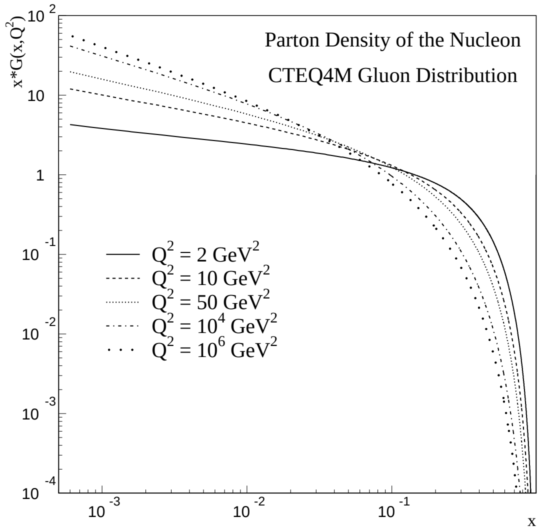

FIG. 5. The gluon parton distribution from CTEQ4M shown at 5 different Q^2 scales.

III. NLO VS LO PDF'S

It is also possible to use leading-order matrix element calculations in the global fits, resulting in leading-order parton distribution functions. Such pdf's are preferred when leading order matrix element calculations (such as Monte Carlo programs like Herwig [7] and Pythia [8] are used. The differences between LO and NLO pdf's, though, are formally NLO; thus, the additional error introduced by using a NLO pdf should not be significant. A comparison of the LO and NLO gluon distribution for the CTEQ4 set is shown in Figure 6 at a Q^2 value of 5 GeV^2 and in Figure 7 at a Q^2 value of 10^4 GeV^2.

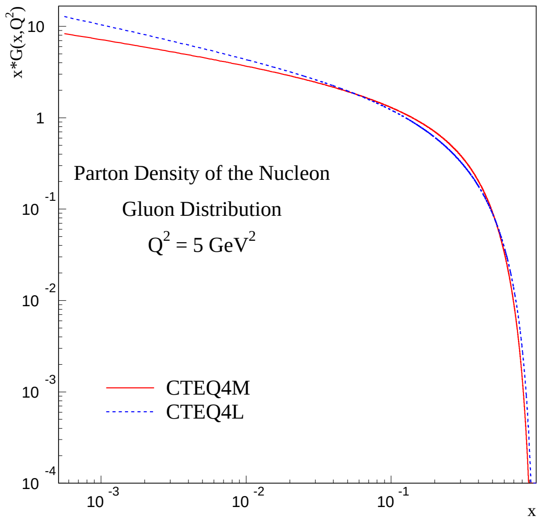

FIG. 6. A comparison of the gluon parton distributions from the CTEQ4 LO and NLO sets plotted at a Q^2 value of 5 GeV^2.

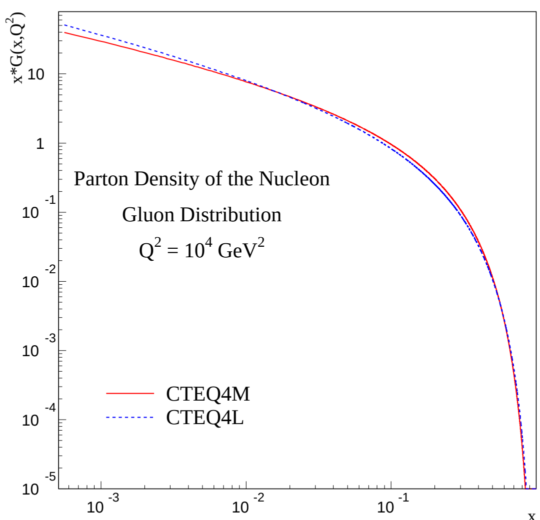

FIG. 7. A comparison of the the gluon parton distributions from the CTEQ4 LO and NLO sets plotted at a Q^2 value of 10^4 GeV^2.

Parton distributions evolve in time as well as Q^2, as new data and theory are added to the global analyses. The evolution (in time and Q^2) for the gluon distribution in the LO pdf's is shown in Figure 8 and Figure 9. It is interesting to note that the gluon distribution in the kinematic region appropriate for production of a light Higgs has not changed appreciably from CTEQ2L to CTEQ4L.

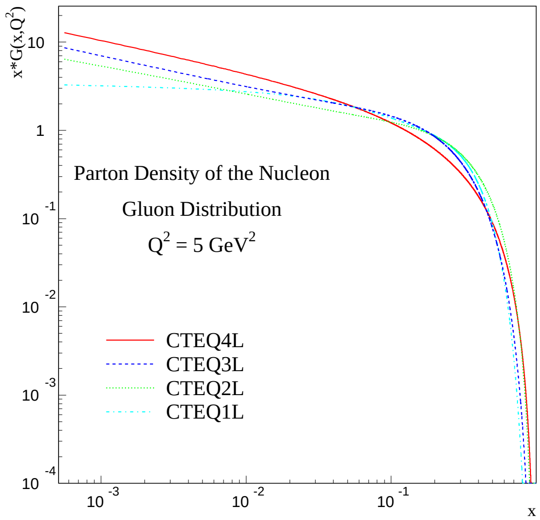

FIG. 8. The gluon parton distributions from the CTEQ1-4 LO sets plotted at a Q^2 value of 5 GeV^2.

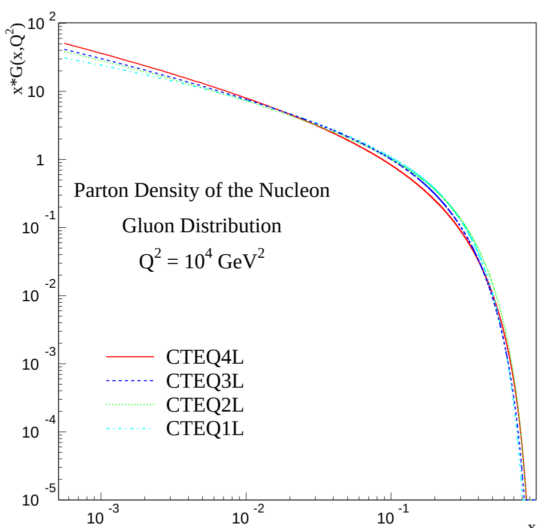

FIG. 9. The gluon parton distributions from the CTEQ1-4 LO sets plotted at a Q^2 value of 10^4 GeV^2.

IV. UNCERTAINTIES ON PDF'S

In addition to having the best estimates for the values of the pdf's in a given kinematic range, it is also important to understand the allowed range of variation of the pdf's, i.e. their uncertainties. The conventional method of estimating parton distribution uncertainties is to compare different published parton distributions. This is unreliable since most published sets of parton distributions (for example from CTEQ and MRS) adopt similar assumptions and the differences between the sets do not fully explore the uncertainties that actually exist. Ideally, one might hope to perform a full error analysis and provide an error correlation matrix for all the parton distributions. (See for example, Ref. [9].) This goal is an admirable one but is difficult to carry out for two reasons. Experimentally, only a subset of the experiments usually involved in global analyses provide correlation information on their data sets in a way suitable for the analysis. Even more important, there is no established way of quantifying the theoretical uncertainties for the diverse physical processes that are used and uncertainties due to specific choices of parameterizations. Both of these are highly correlated. One possibility that has been explored [10] is to invoke only the DIS process, to use only DIS data with the needed correlation information, and to use only those data points at high Q^2 where the theoretical uncertainties are expected to be small. Since these limitations do not take into account the constraints provided by the wide range of data/processes that are thrown away, the uncertainties are clearly unrealistic.

The sum of the quark distributions $(\Sigma(q(x) + \overline{q}(x))$ is, in general, well-determined over a wide range of x and Q^2. As stated above, the quark distributions are predominantly determined by the DIS and DY data sets which have large statistics, and systematic errors in the few percent range ($\pm 3\%$ for $10^{-4} < x < 0.75$). Thus the sum of the quark distributions is basically known to a similar accuracy. The individual quark flavors, though, may have a greater uncertainty than the sum. This can be important, for example, in predicting distributions that depend on specific quark flavors, like the W asymmetry distribution [11] and the W rapidity distribution.

The gluon distribution is the parton distribution that has the greatest uncertainty. The gluon distribution can be determined indirectly at low x by measuring the scaling violations in the quark distributions ($\partial F_2/\partial logQ^2$), but a direct measurement is necessary at moderate to high x. Direct photon production has long been regarded as potentially the most useful source of information on the gluon distribution with fixed target direct photon data, especially from the experiment WA70 [12], being used in a number of global analyses. However, , there are a number of theoretical complications with the use of direct photon data.

The LHC is essentially a gluon-gluon collider and many hadron-collider signatures of physics both within and beyond that Standard Model involve gluons in the initial state. Thus, it is important to estimate the theoretical uncertainty due to the uncertainty in the gluon distribution. Possible sources of information on the gluon distribution and their approximate x range are shown in Figure 10 [6], along with a plot of the MRST gluon pdf.

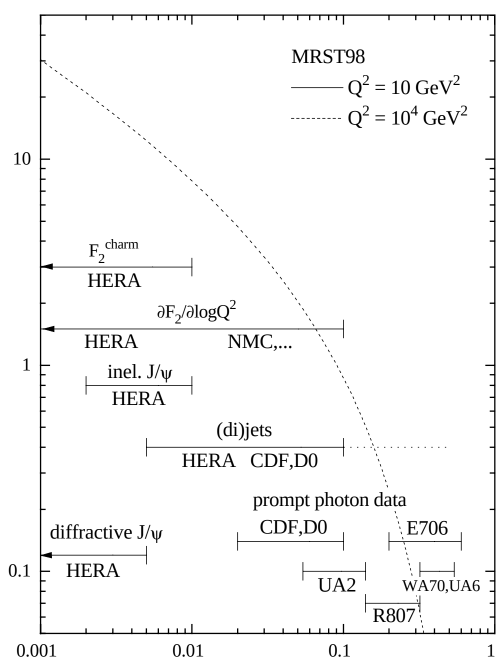

FIG. 10. Sources of information on the gluon distribution.

The momentum fraction of the proton carried by quarks is determined very well from DIS data; at a Q_o value of 1.6 GeV, in the CTEQ4 analysis for example, the momentum fraction carried by quarks is 58% with an uncertainty of $\pm 2\%$. Thus, the momentum fraction carried by gluons is 42% with a similar uncertainty. This constraint is important; if the gluon distribution increases in one x range, momentum conservation forces it to decrease in another x range. The fraction of the proton momentum taken by gluons in a given x range is shown in Table I below. The distribution of gluon momentum fraction is also seen shown in Figure 11. The shift of the gluons to lower x values with increasing Q^2 is evident. The fraction of parton momentum taken by gluons also increases with increasing Q^2.

X Bin	Momentum fraction
10^{-4} to 10^{-3}	0.6%
10^{-3} to 0.01	3%
0.01 to 0.1	16%
0.1 to 0.2	10%
0.2 to 0.3	6%
0.3 to 0.5	5%
0.5 to 1.0	1%

TABLE I. The momentum fraction carried by gluons in a a given x bin at a Q value of 5 GeV.

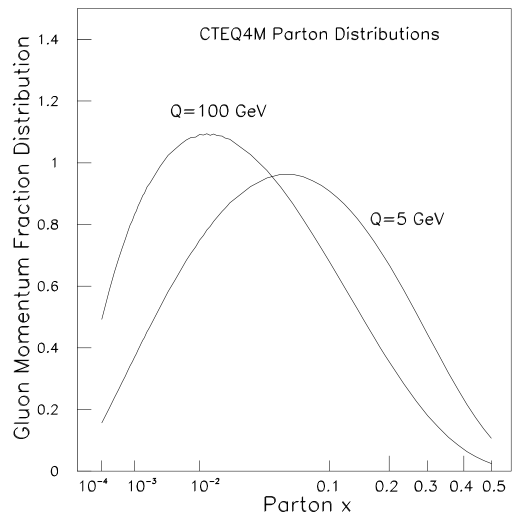

FIG. 11. The fraction of momentum taken by gluons of a given x value for Q = 5 GeV and Q = 100 GeV.

An alternative approach, to those described above, for estimating the uncertainty on the gluon distribution is to systematically vary the gluon parameters in a global analysis and then look for incompatibilities with the data sets that make up the global analysis database. This study has been recently carried out by CTEQ using only DIS and Drell-Yan data where the theoretical and experimental systematic errors are under good control. [13] The CTEQ4 parameterization for the gluon distribution $A_o x^{A1}(1-x)^{A2}(1+A_3 x^{A4})$ was used for this study. The CTEQ4M value of α_s (0.116) was used; the values of A_1, A_2, A_3 and A_4 were systematically varied, each time refitting the other gluon and quark parameters. The gluon pdf's that do not clearly contradict any of the data sets used are shown in Figure 12. Except at larger values of $x (x > 0.2-0.3)$, the variation in the gluon distributions is less than 15% at low values of Q, decreasing to less than 10% at high values. † Note that the DIS and DY datasets used in this analysis do not provide any strong constraints on the gluon distribution

---

†As noted earlier, evolution is the great equalizer for parton distributions.

at high values of x. This study used the CTEQ4 value of α_s. If α_s is varied in the range from 0.113 to 0.122, the gluon distribution varies by 3% for $x < 0.15$.

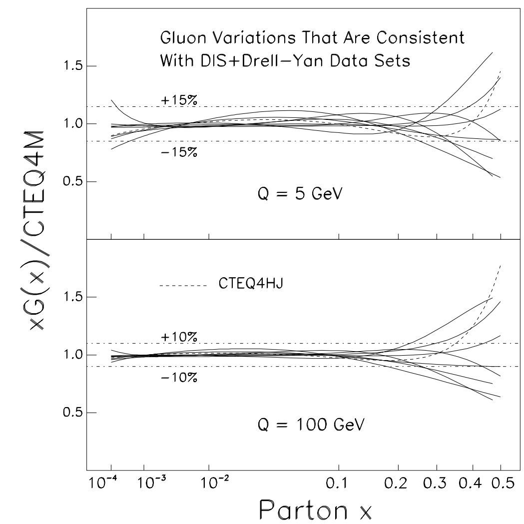

FIG. 12. The ratio of gluon distributions consistent with the DIS and DY data sets to the gluon distributions from CTEQ4M. The gluon distribution from CTEQ4HJ is also shown for comparison.

In order to assess the range of predictions on physics cross sections, it is more important to know the uncertainties on the gluon-gluon and gluon-quark luminosity functions at the appropriate kinematic region (in $\tau = x_1 x_2 = \hat{s}/s$) rather than on the parton distributions themselves. Therefore it is useful to define the relevant integrated parton-parton luminosity functions. The gluon-gluon luminosity function can be defined as:

$$\tau dL/d\tau = \int G(x,Q^2)G(\tau/x,Q^2)dx/x$$

This quantity is directly proportional to the cross section for s-channel production of a single particle and it also gives a good estimate for more complicated production mechanisms. In Figure 13 is shown the range of allowed gluon-gluon luminosities (normalized to the CTEQ4M values) for the variations discussed above. Here, Q^2 is taken to be τs, which naturally takes the Q^2 dependence of the gluon distribution into account as one changes $\sqrt{\tau}$. The top region is for the LHC and the bottom is for the Tevatron. The region of production of a 100-140 GeV Higgs at the LHC is indicated; it lies in the region where the range of variation is $\pm 10\%$. Above an x value of 0.1, the allowed variation grows dramatically (we are squaring the variation shown in Fig. 12 ; this indicates the need for more information about the gluon distribution at large x than provided by the DIS and DY data sets used in this analysis.)

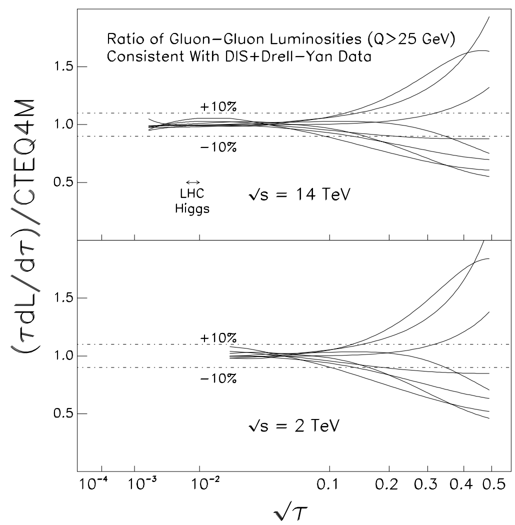

FIG. 13. The rato of integrated gluon-gluon luminosities compared to CTEQ4M is shown as a function of $\sqrt{\tau}$. Shown are examples that are consistent with the DIS+DY data sets used in the fits.

In analogy with the discussion of gluon-gluon luminosities, one can also study the gluon-quark luminosity (again normalized to the CTEQ4M result). The gluon-quark luminosity variations are shown in Figure 14 as a function of $\sqrt{\tau}$ for both the LHC and the Tevatron. (In the plots below, the quark distributions are taken to have no uncertainty; this is not totally unreasonable since the uncertainty on the gluon is considerably larger.)

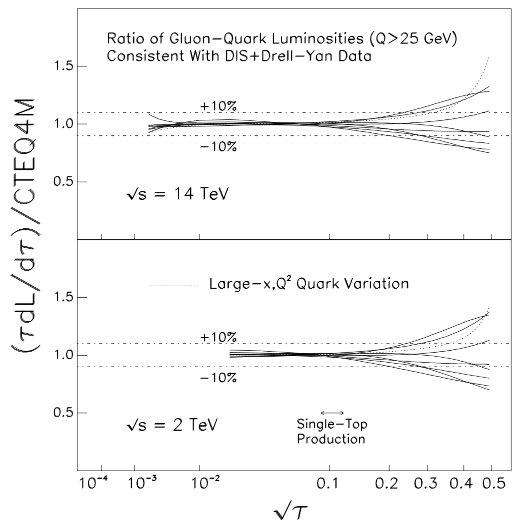

FIG. 14. The ratio of integrated gluon-quark luminosities compared to CTEQ4M is shown as a function of $\sqrt{\tau}$. The examples shown are those consistent with the DIS+DY data sets used in the fits.

The uncertainties on the parton-parton luminosities, as a function of $\sqrt{\tau}$, is summarized in Table II below:

$\sqrt{\tau}$ range	gluon-gluon	gluon-quark
< 0.1	$\pm 10\%$	$\pm 10\%$
$0.1 - 0.2$	$\pm 20\%$	$\pm 10\%$
$0.2 - 0.3$	$\pm 30\%$	$\pm 15\%$
$0.3 - 0.4$	$\pm 60\%$	$\pm 20\%$

TABLE II. The parton-parton luminosity uncertainty as a function of $\sqrt{\tau}$.

V. PROGRESS BEFORE THE LHC TURNS ON

DGLAP-based perturbative QCD calculations have been extremely successful in describing data in DIS, DY and jet production, as well as describing the evolution of parton distributions over a wide range of x and Q^2. From the pdf point-of-view, the primary problem lies in the calculation of fixed target direct photon cross sections; they can serve as a primary probe of the gluon distribution at high x. However, rigorous theoretical treatment of soft gluon effects (requiring both k_T and Sudakov resummation) will be required before the data can be used with confidence in pdf fits.

Differential dijet data from the Tevatron explore a wider kinematic range than the inclusive jet cross section. Both CDF and D0 have dijet cross section measurements from Run I which may also serve probe the high x gluon distribution, in regions where new physics is not expected but where any parton distribution shifts should be observable. The ability to perform such cross-checks is essential.

CDF and D0 will accumulate on the order of 2-4 fb^{-1} of data in Run II (from 2000-2003), a factor of 20-40 greater than the current sample. This sample should allow for more detailed information on parton distributions to be extracted from direct photon and DY data, as well as from jet production. Run III (2003-2007) offers a data sample potentially as large as $30 fb^{-1}$.

H1 and ZEUS will continue the analysis of the data taken with positrons in 1991-97. HERA switched to electron running in 1998 and plans to deliver approximately 60 pb^{-1} in 1999-2000, a factor of X greater than the HERA data sample currently used in the CTEQ5 analysis, for example. In 2000, the HERA machine will be upgraded for high luminosity running, with yearly rates of 150 pb^{-1} expected.

VI. PHYSICS CROSS SECTIONS AT THE LHC AND THE ROLE OF LHC DATA IN PDF DETERMINATION

ATLAS measurements of DY (including W and Z), direct photon, jet and top production will be extremely useful in determining pdf's relevant for the LHC. The data can be input to the global fitting programs, where it will serve to confirm/constrain the pdf's in the LHC range. Again, DY production will provide information on the quark (and anti-quark) distributions while direct photon, jet and top production will provide, in addition, information on the gluon distribution.

The isolated ‡ direct photon cross section at the LHC is shown in Figure 15, along with the predictions of the MRST and CTEQ4M pdf's. [6] In the region plotted, the dominant subprocess is gluon-Compton scattering ($gq \to \gamma q$). Note that the two pdf's lead to similar predictions in this x range.

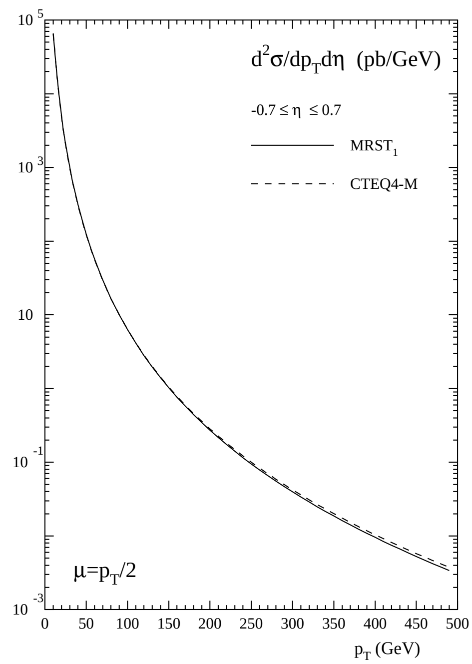

FIG. 15. The isolated direct photon cross section at the LHC along with the NLO QCD predictions using the CTEQ4M and MRST pdf's.

---

‡Using isolation cuts similar to those used by CDF and D0.

The resummed NLO cross section (using the CTEQ4 pdf) for the production of diphotons at the LHC is shown in Figure 16 plotted as a function of the diphoton mass and broken down by subprocess. [15] For relatively low diphoton masses ($< 60 GeV/c^2$), the gg scattering subprocess is dominant and continues to be appreciable out to diphoton masses greater than $100 GeV/c^2$. One point to note is that the resummed gg calculation uses an approximate form for the $gg \to \gamma\gamma g$ matrix element. An implementation of the exact form will increase the contribution of the gg subprocess at higher diphoton masses. [18] Measurements of diphoton production at the LHC will contribute to an improved knowledge of the relevant parton pdf's and parton-parton luminosity functions for the production of the Higgs.

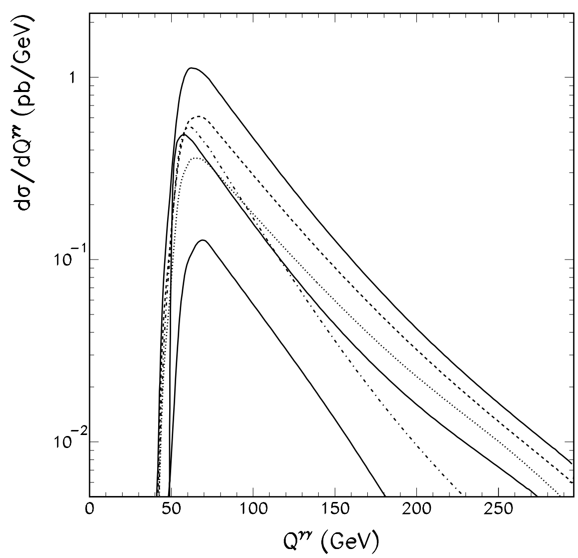

FIG. 16. The invariant mass distribution of photon pairs at the LHC. The total resummed contribution (upper solid), and the resummed $q\bar{q} + qg \to \gamma\gamma X$ (dashed), $q\bar{q} \to \gamma\gamma g$ (dash-dotted), as well as the fragmentation (lower solid) contributions are shown separately. The $q\bar{q} \to \gamma\gamma$ leading order result is shown in the middle solid curve. A p_T cut of 25 GeV/c has been applied to each photon, along with a rapidity cut of 2.5 and a requirement that the leading photon has less than 70% of the p_T of the photon pair.

For comparison purposes, the diphoton cross section at the Tevatron is shown, plotted in a similar manner, and compared to the CDF data from Run 1B. [16] For masses less than $30GeV/c^2$, the gg subprocess dominates and remains appreciable out to mass values of $50GeV/c^2$ or so. The same comment about the approximate form for the $gg \to \gamma\gamma g$ matrix element applies here also. Note that the much higher statistics for Run II will allow both the gg luminosity and the physics formalism for diphoton production to be probed with much higher statistics.

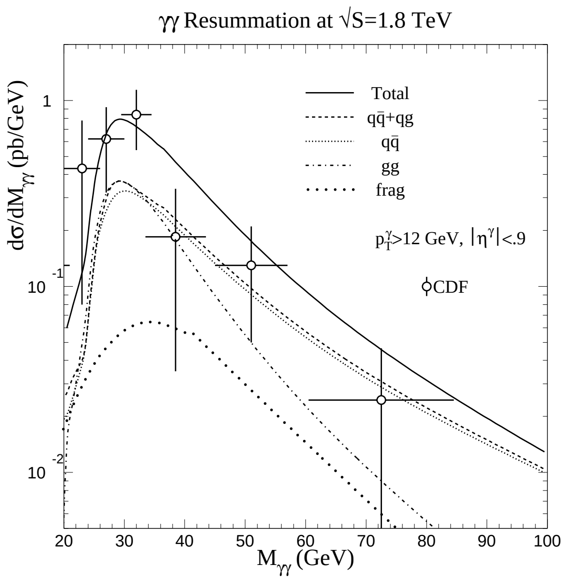

FIG. 17. The predicted distribution for the invariant mass of the photon pair from the resummed calculation compared to the CDF data, with the CDF cuts imposed in the calculation.

The resummed NLO cross section for the production of the SM Higgs is shown in Figure **??** plotted as a function of the Higgs mass, broken down by subprocess and using the CTEQ4 pdf. [17] As can be seen, the gg subprocess is far more dominant for the case of Higgs production than in the case of diphoton production.

A comparison of jet production at the Tevatron and the LHC is shown in Figure 18. [6] The "reach" at the LHC is to jet E_T values of approximately 4 TeV/c. There are noticable differences between the predictions using the 3 pdf's listed. This difference is more evident in the linear comparison shown in Figure 19. [6] An E_T value of 4 TeV/c corresponds to an x_T value of about 0.57. At this x_T value, the CTEQ4HJ pdf prediction is about 30% higher than the CTEQ4M prediction, while the MRST prediction is about 7% smaller. Note that the size of the relative deviations is very similar at the LHC and Tevatron.

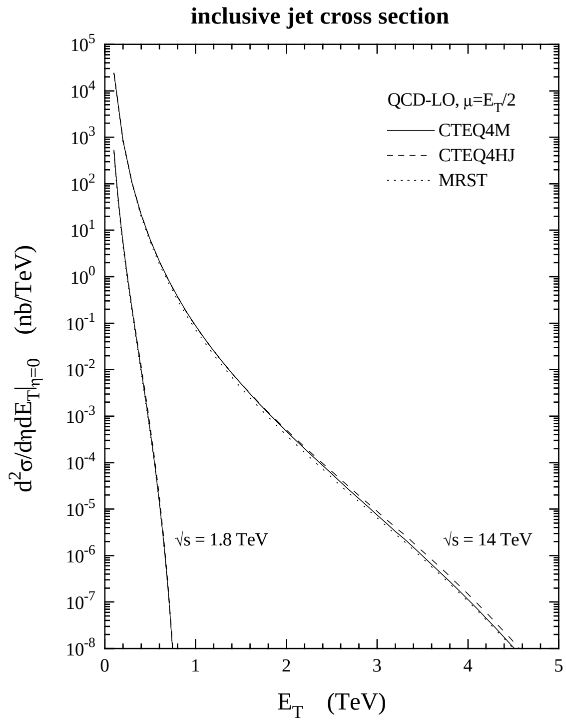

FIG. 18. The inclusive jet cross sections at a rapidity of 0 for both the Tevatron and the LHC.

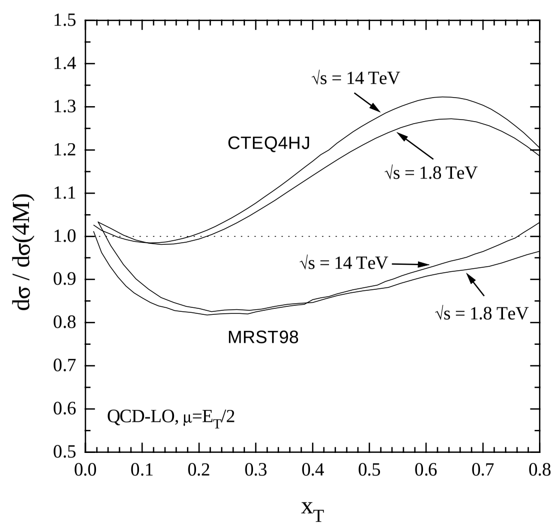

FIG. 19. A comparison of the predictions for the inclusive jet cross sections at a rapidity of 0 for both the Tevatron and the LHC using three different pdf's.

The subprocesses responsible for jet production at the LHC are shown in Figure 20, similar to the subprocess plot for the Tevatron. The relative fraction of each subprocess is very close to the fraction at the Tevatron, if the fractions are plotted as a function of x_T. Gluon-gluon scattering dominates at the lowest values of E_T, with gluon-quark dominating at moderate values of E_T and quark-quark at the highest values.

FIG. 20. The relative proportion of processes contributing to jet production at the LHC.

The cross sections for the production of W^+ and W^- at the LHC are symmetric with respect to $\eta = 0$. This is in contrast to the asymmetry that is observed at the Tevatron due to $\overline{p}p$ collisions rather than pp collisions. The W^+ production cross section is larger than the W^- production cross section at the LHC; in addition there is a great deal of information on parton distribution densities that can be obtained from the $W^{+,-}$ rapidity distributions. For example, in Figure 21, the $W^{+,-}$ rapidity distributions are shown along with the parton kinematics probed at rapidites of 0 and 3. [6]

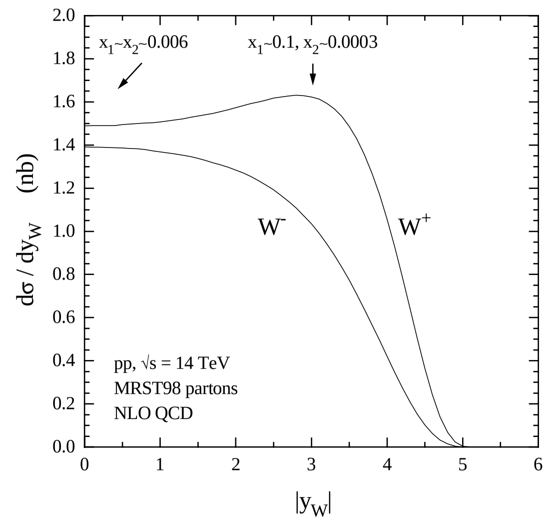

FIG. 21. The $W^{+,-}$ rapidity distributions for pp collisions at the LHC.

Another possibility that has been suggested is to directly determine parton-parton luminosities (and not the parton distributions per se) by measuring well-known processes such as W/Z production. [19] This technique would not only determine the product of parton distributions in the relevant kinematic range but would also eliminate the difficult measurement of the proton-proton luminosity. It may be more pragmatic, though, to continue to separate out the measurements of parton pdf's (though global analyses which may contain LHC data) and of the proton-proton luminosity. The measurement of the latter quantity can be pegged to well-known cross sections, such as that of the W/Z, as has been suggested for the Tevatron.

[1] These issues are explored in more depth in the ATLAS note "LHC Guide to Parton Distribution Functions and Cross Sections"; also for a recent review of QCD physics, see J. Huston, plenary talk on QCD at the ICHEP conference in Vancouver ("QCD at High Energies"); **hep-ph/9901352**.

[2] H.L. Lai, J. Huston et al., **hep-ph/9903282**.

[3] A.D. Martin, R.G. Roberts, W.J. Stirling and R. Thorne, *Eur. Phys. J.* **C4**, 463 (1998).

[4] H.L. Lai, J. Huston et al., *Phys. Rev.* **D55**, 1280 (1997), **hep-ph/9606399**.

[5] See, for example, the plenary talk given by Y. Dokshitzer at the ICHEP conference in Vancouver, **hep-ph/9812252**.

[6] I would like to thank James Stirling for providing these plots; most were taken from his talk on LHC physics at the Feb 1998 workshop on LHC Physics Processes.

[7] G. Marchesini et al., **hep-ph/9607393**.

[8] T. Sjostrand, **hep-ph/9508391**.

[9] W.T. Giele, Stephane Keller, *Phys. Rev.* **D58**, (1998), **hep-ph/9803393**.

[10] alekhin reference

[11] CDF Collaboration, F. Abe et al., *Phys. Rev. Lett.* **81**, 5754 (1998), **hep-ex/9809001**.

[12] M. Bonesini et al., *Z. Phys.* **C38**, 371(1988); *ibid.* **C37**,535(1988); *ibid.* **C37**, 39.

[13] J. Huston et al., *Phys. Rev.* **D58** (1998), **hep-ph/9801444**.

[14] J.Huston et al., *Phys.Rev.Let.* **77**, 444(1996).

[15] C. Balazs et al., **hep-ph/9810319**, accepted by *Phys. Rev.* D.

[16] C. Balazs et al., *Phys. Rev.* **D57**, 6934(1998), **hep-ph/9712471**.

[17] lhc higgs calculation

[18] C. Balazs, private communication.

[19] M. Dittmar, F. Pauss, D. Zuercher, *Phys. Rev.***D56**, 7284; **hep-ex/9705004**.